Spectroscopic Fingerprints of Work-Function-Controlled Phthalocyanine Charging on Metal Surfaces

Patrizia Borghetti,*,†,‡ Afaf El-Sayed,‡,§ Elizabeth Goiri,†,‡ Celia Rogero,†,‡ Jorge Lobo-Checa,‡ Luca Floreano,∥ Jose Enrique Ortega,*,†,‡,§ and Dimas G. de Oteyza*,†,‡

†Donostia International Physics Center, Paseo Manuel Lardizabal 4, San Sebastián, Spain, ‡Centro de Fisica de Materiales (CSIC-UPV/EHU)-Materials Physics Center (MPC), San Sebastián, Spain, §Dpto. Física Aplicada I, Universidad del Pais Vasco, San Sebastián, Spain, and ∥CNR-IOM, Laboratorio Nazionale TASC, Basovizza SS-14 Km. 163.5, Trieste, Italy

ABSTRACT The electronic character of a π-conjugated molecular overlayer on a metal surface can change from semiconducting to metallic, depending on how molecular orbitals arrange with respect to the electrode's Fermi level. Molecular level alignment is thus a key property that strongly influences the performance of organic-based devices. In this work, we report how the electronic level alignment of copper phthalocyanines on metal surfaces can be tailored by controlling the substrate work function. We even show the way to finely tune it for one fixed phthalocyanine–metal combination without the need to intercalate substrate-functionalizing buffer layers. Instead, the work function is trimmed by appropriate design of the phthalocyanine's supramolecular environment, such that charge transfer into empty molecular levels can be triggered across the metal–organic interface. These intriguing observations are the outcome of a powerful combination of surface-sensitive electron spectroscopies, which further reveal a number of characteristic spectroscopic fingerprints of a lifted LUMO degeneracy associated with the partial phthalocyanine charging.

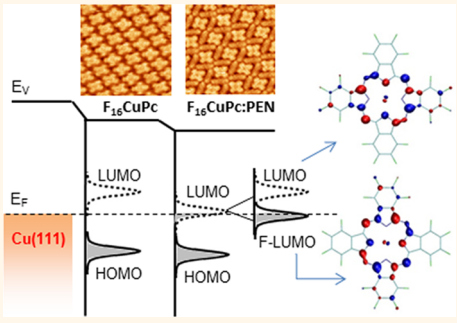

KEYWORDS: metal–organic interfaces · energy-level alignment · molecular blends · photoemission · NEXAFS

Energy-level alignment at heterointerfaces plays an essential role in the functionality of charge injection devices, such as organic solar cells, where the efficiency is largely determined by the relative band edge positions of all its constituents. By way of example, band alignment at the metal/semiconductor interface critically affects the contact resistance, which often limits device performance.[1] In fact, an appropriate level alignment may drive the formation of hybrid interface states at the Fermi energy, trigger significant charge transfer, and lower interface potential barriers.[2,3] Electrical doping[4] and/or interface engineering[1,5−8] are thus essential to optimize the relative energies of the electronic states involved in the conduction within each of the materials: (i) the states around the Fermi level in the metal and (ii) the valence or conduction bands in the semiconductor.[9,10] For the particular case of organic semiconductors, upon which increasingly high hopes are being placed as future active components of a variety of devices, the critical states correspond to the highest occupied (HOMO) and lowest unoccupied molecular orbitals (LUMO). Their alignment with respect to the substrate's Fermi level has therefore been extensively studied over the past decades for many molecule–metal combinations. Initially, it was assumed that the energetics was governed by vacuum-level alignment according to the Schottky–Mott model. Within this model, for a given molecule with specific ionization potential and electron affinity, the charge injection barriers are simply defined by the electrode's work function. It was soon found, however, that much more complex processes are involved, including the generation of interface dipoles, charge transfer, or interface hybridizations,[2,3,11,12] which furthermore become increasingly intertwined as the system's complexity rises in, for example, molecular blends.[13−22] For all that, the electrode's work function remains, although in a

* Address correspondence to patrizia_borghetti@ehu.es, enrique.ortega@ehu.es, d_g_oteyza@ehu.es.

Received for review October 22, 2014 and accepted November 26, 2014.

Published online November 26, 2014
10.1021/nn5060333

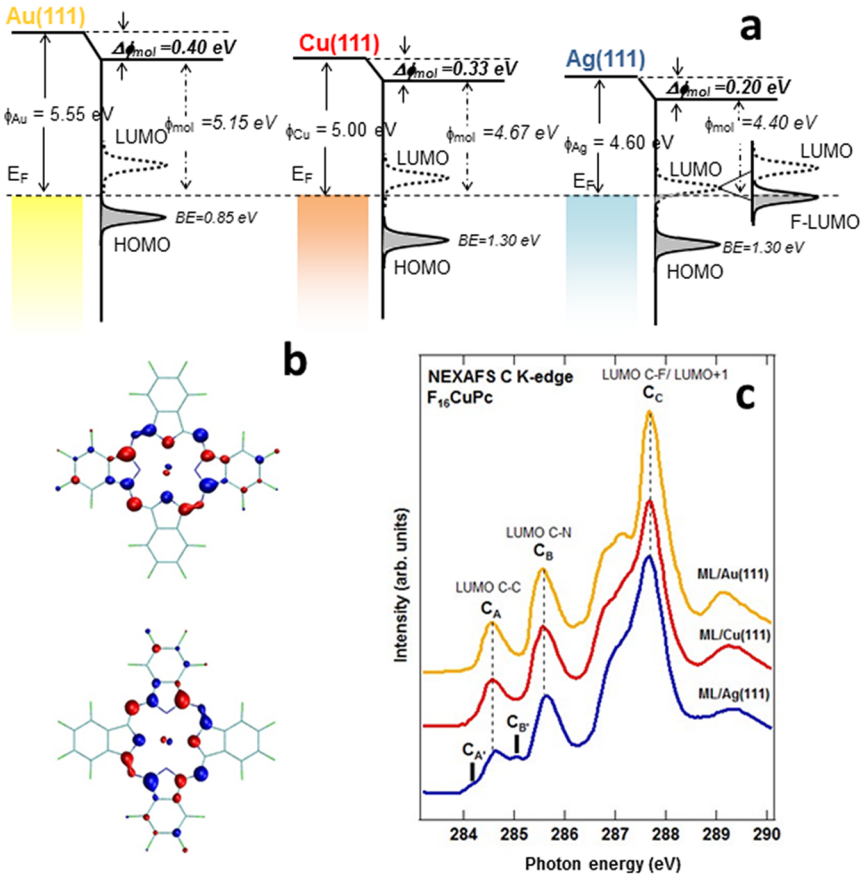

Figure 1. (a) Energy-level diagram of a $F_{16}CuPc$ monolayer on Au(111), Cu(111), Ag(111) based on the present results. In $F_{16}CuPc$/Ag(111), E_F crosses the low-energy tail of the LUMO level, leading to a partial charge transfer from substrate to molecule. As a consequence, the two-fold degeneracy of $F_{16}CuPc$ LUMO is lifted, with one of the split states partially occupied. (b) Density of states of the double degenerate e_g LUMO levels of the isolated $F_{16}CuPc$ molecule (extracted from the calculations of ref 32). The two orbitals are equal but rotated by 90° with respect to each other. (c) P-polarization NEXAFS C K-edge spectra of $F_{16}CuPc$ monolayers on the three surfaces. Transitions to $F_{16}CuPc$ LUMO from the C 1s core level at the C−C, C−N, and C−F sites are indicated on top of the corresponding peaks. For $F_{16}CuPc$/Ag(111), the presence of additional components due to the LUMO splitting are marked.

less predictable manner, a key parameter with which to influence the energy-level alignment. Most importantly, the work function can be easily modified experimentally, typically by changing the substrate material or the surface orientation or by additional surface functionalization.

In this work, we apply this concept to phthalocyanine-based metal−organic interfaces. Today, copper phthalocyanine, CuPc, an archetypal heteroaromatic dye, and its fluorinated counterpart, $F_{16}CuPc$,[23] are widely studied due to their electronic properties, processing flexibility, and the promising efficiencies of phthalocyanine-based optoelectronic devices. Using a thorough electron spectroscopy approach, we characterize the electronic levels of copper phthalocyanines at the interface with coinage metals. As a result of the decreasing work function when changing from Au(111) through Cu(111) to Ag(111), we observe a tunable energy-level alignment, including a controllable charge transfer to the molecular LUMO. Our spectroscopic analysis reveals that transferring charge from the substrate lifts the LUMO degeneracy, breaking the four-fold symmetry of the phthalocyanine. Most remarkably, we show that this charge transfer into the LUMO can be tuned even at the very same metal−organic interface by making use of the supramolecular environment-dependent work function in molecular blends.[19,20]

RESULTS

The different interface energy-level alignment of $F_{16}CuPc$ monolayers on various coinage metal surfaces is summarized schematically in Figure 1a. From photoemission experiments described in more detail below, we extract the HOMO level positions, as well as the work functions of Au(111), Cu(111), and Ag(111) surfaces before and after being covered by full $F_{16}CuPc$ monolayers (ML). The latter include the interface dipoles and turn out to be the truly relevant magnitudes. Unless important chemical interactions set in,[3] interface dipoles typically scale linearly with the substrate's original work function,[24] with proportionality constants ranging from 1 for a Fermi level pinning scenario to 0 as a vacuum-level pinning scenario is approached.[25] Here, with interface dipoles of 0.4, 0.33, and 0.2 eV for Au(111),

Cu(111), and Ag(111) substrates, respectively, their final effective work functions amount to 5.15 ± 0.03, 4.67 ± 0.03, and 4.40 ± 0.03 eV. In this probed range, the Fermi level (E_F) excursion within the molecular semiconducting gap reaches neither the HOMO level nor its high-energy tail. The LUMO energies were not accessed experimentally but can be roughly estimated by summing the HOMO−LUMO gap energy to that of the HOMO. The reported gap value from combined direct and inverse photoemission on F_{16}CuPc multilayer films amounts to 1.8 eV as measured from peak-onset to peak-onset.[11,26] Because HOMO−LUMO gaps are considerably reduced by stronger image charge effects in monolayers on metals,[12] we assume this value corresponds approximately to the peak-to-peak gap of F_{16}CuPc monolayers on metal surfaces. This implies that in our experiments E_F is roughly centered in the gap for the Au(111) case, approaching the LUMO as the work function is reduced. In fact, photoemission data show that on Ag(111) E_F crosses the low-energy tail of the LUMO level, inducing a partial charge transfer from substrate to molecule. As shown in Figure 1a and in analogy to the previously reported findings upon charging of the closely related CuPc,[27] the two-fold degeneracy of the F_{16}CuPc e_g LUMO levels (displayed in Figure 1b), is thus lifted, likely by a Jahn−Teller effect, splitting into a still empty LUMO and a partially filled F-LUMO.

The lifted degeneracy of LUMO levels is best observed by probing the unoccupied molecular orbitals by means of NEXAFS. Spectra of the C K-edge of F_{16}CuPc monolayers on the three different surfaces are displayed in Figure 1c. On Au(111) and Cu(111), the spectra closely resemble that of a multilayer,[23] indicating that contact with these surfaces does not significantly alter the unoccupied states of F_{16}CuPc. By contrast, on Ag(111), significant modifications are found in the low-energy part of the spectrum: two additional components ($C_{A'}$ and $C_{B'}$) appear at the low photon energy side of peaks C_A and C_B. According to previous findings on F_{16}CuPc thick films,[28] C_A and C_B correspond to transitions from the C 1s core levels on the C−C phenyl and C−N pyrrole sites, respectively, to the LUMO. A plausible explanation for the spectral changes is the association of the new additional components at lower photon energy ($C_{A'}$ and $C_{B'}$) and the main absorption lines (C_A and C_B) with transitions into the low- and high-energy components of the split LUMO levels, respectively. The partial occupation of the lower energy LUMO level (F-LUMO) also agrees with the lower intensity of the new components, while the absence of similar fingerprints on subsequent resonances is explained by the convolution with absorption transitions onto higher energy unoccupied orbitals unaffected by the Jahn−Teller distortion.[28]

Comparison of the valence band spectra of F_{16}CuPc on Au(111) and Ag(111), displayed in Figure 2a, supports the above-described scenario. That is, lowering the work function when going from Au(111) to Ag(111) not only increases the HOMO binding energy from 0.85 to 1.30 eV but also causes a partial filling of the LUMO level on Ag(111). This is observable as an increase in the photoemission intensity close to the Fermi level with respect to the signal on the clean substrate, whereas it is absent for F_{16}CuPc on Au(111). Fitting of the spectrum on Ag(111) (included in Figure 2a) renders a F-LUMO centered at 0.15 eV and clearly truncated at the Fermi edge, indicative of the partial filling that leaves another part of the level empty and accessible to NEXAFS experiments.

The associated N K-edge NEXAFS spectra taken under p- and s-polarization on F_{16}CuPc monolayers on Au(111) and Ag(111) are displayed in Figure 2b. The most remarkable difference among both substrates is the appearance on Ag(111) of a clear shoulder $N_{A'}$ at $h\nu$ = 397.5 eV, just at the low-energy side of the first main peak N_A associated with transitions into the LUMO. This feature $N_{A'}$ is observed neither in the spectra on Au(111) nor in the multilayer and is ascribed, as in the C K-edge spectra (Figure 1c), to the split and partially filled LUMO level. As a result of the partial charge transfer, the total intensity obtained by summing the contributions of N_A and $N_{A'}$ on Ag(111) is still 15% less than the intensity of N_A on Au(111). Considerable spectral modifications on Ag(111) are also detected in the photon energy range between 399 and 403 eV, including a shift of about 0.3 eV to lower photon energy for the band N_B and a broadening toward the low photon energy side of band N_C (ascribed in analogy to CuPc to transitions into the LUMO+1 and LUMO+2, respectively).[29] The changes are analogous to those observed on CuPc upon K[29] and Rb[30] doping and thus provide further support for our proposed partial LUMO filling scenario. Spectral changes appear solely under p-polarization, underlining their origin in π^* orbitals. Moreover, the complete quenching of the π^* transitions in s-polarization, which has been measured also for the C K-edge, indicates a flat absorption configuration for the F_{16}CuPc plane on both Au(111) and Ag(111) surfaces, as observed also by scanning tunneling microscopy.[31,32] The equally flat orientation adopted by molecules on both surfaces thus guarantees that the differences observed between the NEXAFS spectra of the two systems stem from changes in the electronic structure rather than from a modified molecular orientation.

On Cu(111), F_{16}CuPc NEXAFS measurements at the C K-edge (Figure 1c) and N K-edge (Figure S1) show very similar spectral line shapes to those on Au(111), suggestive of an absence of charge transfer from substrate to molecule. Indeed, no intensity close to E_F is found in valence band photoemission spectra of F_{16}CuPc/Cu(111) (Figure 3a). HOMO−LUMO gap values may show minor deviations depending on the substrates and the associated gap renormalization

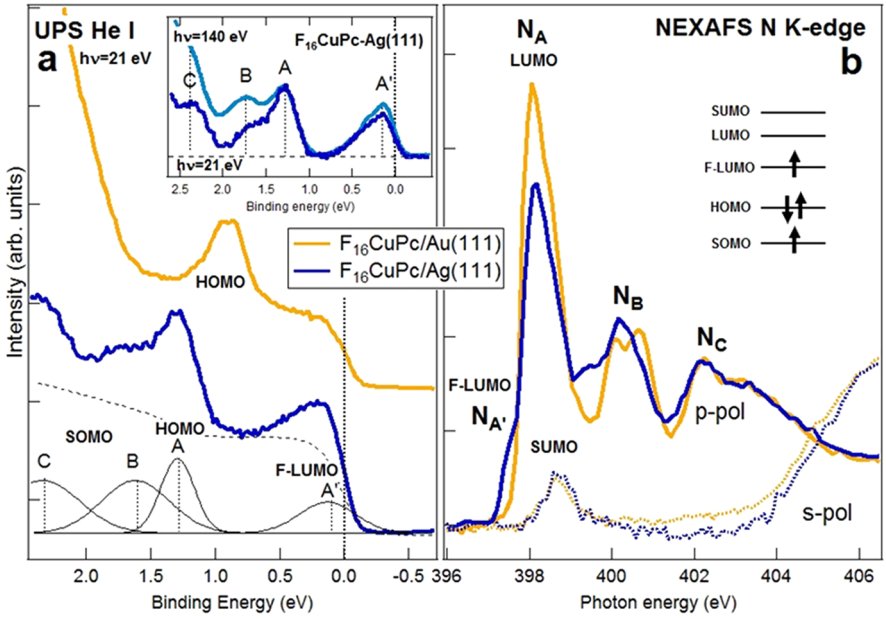

Figure 2. (a) Valence band spectra of F_{16}CuPc/Au(111) (yellow line) and F_{16}CuPc/Ag(111) (dark blue line) measured with $h\nu$ = 21 eV. For the latter, the fit components (black solid lines) and the Shirley background convoluted with a Fermi step function (black dashed line) obtained from the fitting procedure are shown in the bottom part. Inset: Valence spectra of F_{16}CuPc/Ag(111) taken with $h\nu$ = 21 eV (dark blue line) and $h\nu$ = 140 eV (light blue line) after subtracting the corresponding clean reference spectra. (b) NEXAFS N K-edge spectra of F_{16}CuPc/Au(111) (yellow line) and F_{16}CuPc/Ag(111) (dark blue line) taken under p-polarization (solid lines) and s-polarization (dashed lines). Inset: Indicative energy scheme of F_{16}CuPc energy levels on Ag(111), as deduced from present data.

factors such as hybridization or adsorption heights.[12] Nevertheless, from the similar HOMO binding energy and the relatively close work functions of F_{16}CuPc/Cu and F_{16}CuPc/Ag, we expect the F_{16}CuPc/Cu LUMO to be close to E_F (Figure 1a). As recently reported, one way to fine-tune the sample's work function and thereby the energy-level alignment at the molecule/metal interface is to mix molecular species whose associated interface dipoles on a given surface differ significantly.[19] This is typically the case, for example, with molecules of complementary donor and acceptor character.[19,33] In the case of F_{16}CuPc, the molecular levels can be rigidly shifted to higher binding energies by mixing them with pentacene (PEN) molecules. On Cu(111), F_{16}CuPc:PEN monolayer blends with a 1:2 stoichiometry form a particularly stable and easy to prepare crystalline structure, as determined by scanning tunneling microscopy (Figure 3c).[19] In the blends, changes in F_{16}CuPc's energy-level alignment may arise from the new supramolecular environment and the new intermolecular interactions with the surrounding H-bonded PEN molecules.[19,21,34,35] However, as recently shown, those changes may be dominated (compensated or even reversed) by changes in the work function, which for the blends corresponds in a good approximation to a weighted average of the work functions associated with layers of each of the molecules separately.[19,20] The work function of the 1:2 blend on Cu(111) is slightly lower than that of F_{16}CuPc/Ag(111) (ϕ = 4.28 ± 0.03 *vs* 4.40 ± 0.03 eV, Figure 1a and Figure 3c), and thus we expect comparable or even stronger interfacial charge transfer effects in the case of the 1:2 blend on Cu.

To confirm this assumption, valence band photoemission and NEXAFS spectra were measured for the blend. Figure 3a shows valence band spectra of the 1:2 blend grown by sequential deposition of 0.5 ML of PEN followed by 0.5 ML of F_{16}CuPc (note that due to the different molecular sizes a 1:1 ratio in surface area coverage corresponds to a 1:2 stoichiometry), although equivalent results can be obtained by co-depositing the two molecular species. The valence band spectrum of 0.5 ML of PEN displays two peaks at 0.65 eV (A) and 1.35 eV (B). By adding 0.5 ML of F_{16}CuPc, peak B increases in intensity due to the additional overlapping emission of the F_{16}CuPc HOMO, while a noticeable intensity A′ appears at the low binding energy side of PEN's peak A. To highlight this feature, we subtract the spectrum of 0.5 ML PEN from that of the 1:2 blend (black line in bottom part of Figure 3a) and compare it to the pure F_{16}CuPc monolayer spectrum after subtraction of the Cu(111) reference spectrum (red line in bottom part of Figure 3a). From this analysis, it is evident that the new structure appearing at about 0.30 eV is characteristic neither of the PEN nor of F_{16}CuPc pure layers but arises from mixing the two species. In view of the results on F_{16}CuPc/Ag(111), we ascribe this new feature to the partially filled F_{16}CuPc LUMO (F-LUMO). Probing the unoccupied molecular orbitals, NEXAFS N K-edge spectra on Cu(111) change substantially if we compare pure F_{16}CuPc layers with F_{16}CuPc:PEN blends (Figure 3b). As occurred for F_{16}CuPc on Ag(111), in the blends on

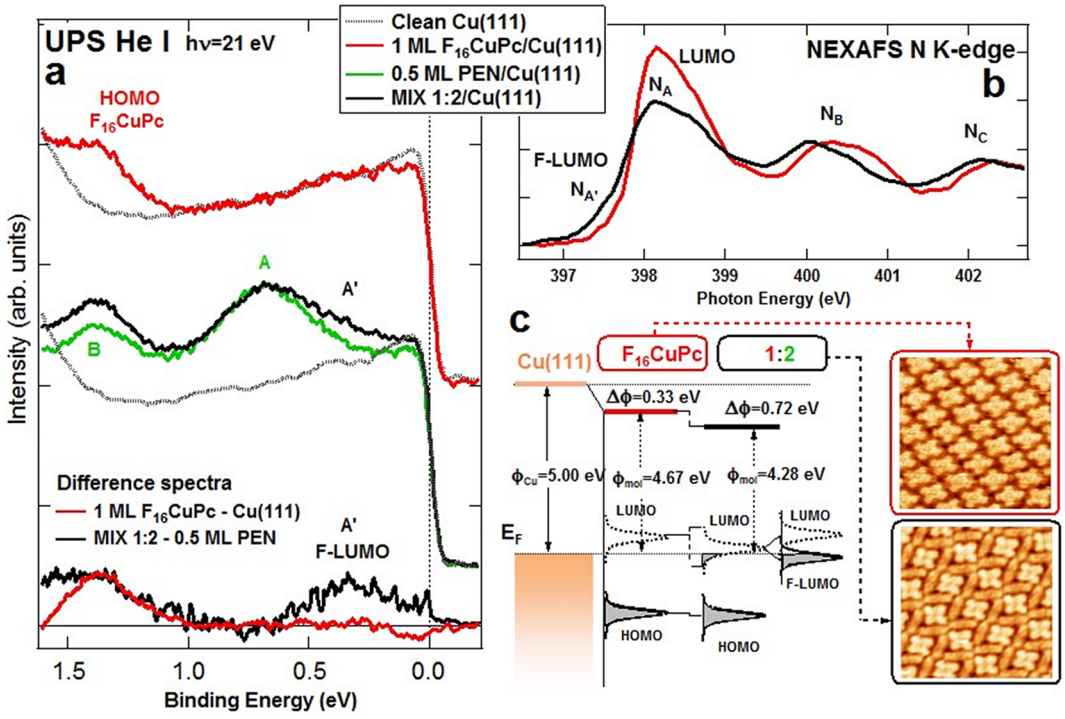

Figure 3. (a) Valence band spectra of a monolayer of F_{16}CuPc/Cu(111) (top red line), 0.5 ML of PEN/Cu(111) (middle green line), and the subsequent 1:2 blend of F_{16}CuPc:PEN/Cu(111) (middle black line). Cu(111) clean reference spectra are also shown (gray dotted lines). The bottom part displays the F_{16}CuPc/Cu(111) spectrum after subtracting the clean reference spectrum (red line) and the 1:2 blend spectrum after subtracting the 0.5 ML PEN spectrum (black line). In order to account for the reduced amount of F_{16}CuPc, the spectrum of the mix has been doubled in intensity, which consistently results in an equal intensity value for the F_{16}CuPc HOMO peak. (b) NEXAFS N K-edge spectra of F_{16}CuPc/Cu(111) (red line) and the 1:2 blend of F_{16}CuPc:PEN/Cu(111) (black line) acquired in p-polarization. For both systems, the schematic energy-level diagram and STM images (9×9 nm^2, $V = -0.7$ V, and $I = 0.7$ nA) in constant current mode are presented in panel (c). As sketched, the work function (ϕ) reduction in the 1:2 blend leads to the partial charge transfer from substrate to F_{16}CuPc molecule and hence to the splitting of the two-fold degenerate F_{16}CuPc LUMO levels.

Cu(111), an absorption intensity $N_{A'}$ appears at the low-energy side of the main peak N_A, which in turn appears significantly reduced; N_B shifts down in energy, and N_C broadens at the low photon energy side. All the above details are in line with a partial filling of the LUMO level and the consequent lifting of its degeneracy as displayed schematically in Figure 3c.

It is worth mentioning that the new peak emerging in the valence band spectrum of the 1:2 blend on Cu(111) is detected at 0.15 eV higher binding energy than the corresponding peak of F_{16}CuPc/Ag(111). This is in fair agreement with the difference in work function measured for the two systems, which underlines the fundamental role of vacuum-level shifts in moving F_{16}CuPc frontier orbitals below E_F and further demonstrates the possibility of fine-tuning charge transfer across phthalocyanine−metal interfaces by work function manipulation. Indeed, in accordance with the smaller work function value and larger binding energy of the F-LUMO feature, a stronger degree of LUMO filling is deduced for the blend on Cu(111), which is further confirmed by a stronger decrease in intensity in the NEXAFS N K-edge spectra of peaks N_A and $N_{A'}$ for the 1:2 blend on Cu(111) than for those on F_{16}CuPc/Ag(111) (see Supporting Information, Figure S1).

Core levels are sensitive to the charge state of the atoms from which they originate and consequently to molecular charging. Besides, they represent the initial states for the electronic transitions measured in NEXAFS experiments and thus have direct impact on those spectra. To deepen our understanding of the above-described findings, we have measured N 1s and C 1s core-level spectra of each of the systems discussed above and summarized them, along with their corresponding fits, in Figure 4. While F_{16}CuPc comprises two non-equivalent N atom sites and four C atom sites, for monolayers on Au(111), as well as for multilayers, satisfactory fits can be obtained by using only one component for the N 1s spectrum and three components for the C 1s spectrum (together with their associated satellites). The latter correspond to C atoms bonded solely to C (C−C), C atoms in the pyrrole rings bonded to N (C−N), and C atoms bonded to F (C−F), in order of increasing binding energy as the partial electron charge on the atoms is reduced being bound to species of increasing electronegativity.[19,23,28] The fitted integrated intensity ratio for peaks C−C/C−N/C−F agrees well with the expected 1:1:2 ratio for this molecule. For F_{16}CuPc on Cu(111), the spectra can be fitted with a similar model (Figure 4), albeit with broader

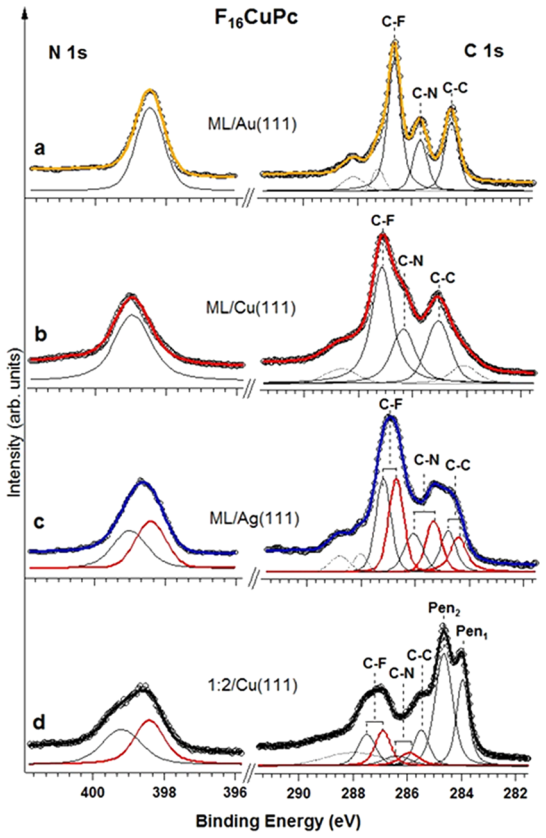

Figure 4. X-ray photoemission spectra in the N 1s (left panels) and C 1s (right panels) core-level regions of F_{16}CuPc/Au(111) (a), F_{16}CuPc/Cu (111) (b), F_{16}CuPc/Ag(111) (c), and 1:2 blend of F_{16}CuPc:PEN/Cu(111) (d). Experimental points (markers) are superimposed to fit spectra (solid line). In (c) and (d), split-off components (in red) arise as a consequence of the more efficient screening of the partially filled LUMO.

components stemming from a stronger molecule–substrate hybridization, previously concluded also from the closer molecule–substrate adsorption distance measured with X-ray standing waves.[32,36,37] As occurred with the HOMO, core levels are shifted by 0.5 eV to higher binding energy with respect to F_{16}CuPc on Au(111), which is consistent with the difference in work function measured for the two interfaces (Figure 1a). More important changes are observed for the F_{16}CuPc N 1s and C 1s core-level spectra as its LUMO gets partially filled in F_{16}CuPc/Ag(111) and F_{16}CuPc:PEN/Cu(111). In these cases, the fitting procedure requires additional components to provide satisfactory results, evidencing an unambiguous splitting into two components with similar area behind the overall strongly broadened spectra. With this splitting effect being related to the partial charging of the F_{16}CuPc LUMO, it is strongest for the system with larger charge transfer, F_{16}CuPc:PEN/Cu(111). The splitting's physical origin will be addressed in the discussion.

Finally, on the closely related sister molecule CuPc, the same phenomenology is observed. Both molecules share similar electronic attributes, except for the larger electron affinity and ionization potential brought about by the molecular fluorination in F_{16}CuPc.[23,32,38] However, the typically smaller interface dipole generated by fluorinated molecules[19,33] leaves F_{16}CuPc and CuPc with a comparable interfacial energy-level alignment. As a consequence, the same spectral changes are observed when comparing CuPc's valence band (Figure 5a) and core-level photoemission (Figure 5c), as well as NEXAFS spectra (Figure 5b), on Au(111) and Ag(111). On Ag(111), unambiguous intensity appears close to E_F in the valence band photoemission spectra that corroborates partial filling of the LUMO (Figure 5a), in agreement with previous studies.[39] Core-level spectra evidence their splitting into two components (Figure 5c), and in N K-edge NEXAFS spectra, a clear shoulder $N_{A'}$ is observed at the low-energy side of the N_A LUMO resonance; the band N_B is shifted down in energy, and band N_C is broadened. Altogether, we conclude the same scenario as for F_{16}CuPc: as the work function is reduced in Ag(111), partial filling of the CuPc LUMO levels takes place and lifts their degeneracy (Figure 5d). Noteworthy for our following discussion, the F-LUMO state is observed already at the submonolayer coverage (0.25 and 0.55 ML) and grows in intensity as the coverage increases up to the ML (see Supporting Information, Figure S2). Once the ML is formed, a further deposition of CuPc induces this peak to decrease, being completely absent at the nominal coverage of about 4 ML. Concurrently, the N 1s and C 1s spectra in the sub-ML to ML coverage regime are satisfactorily fitted by doubling the number of components, while at higher coverages, the fit components simply reflect the stochiometry of the molecule (see Supporting Information, Figure S2).

DISCUSSION

The combined photoemission and absorption analysis of organic/metal interfaces becomes extremely precise and powerful when carried out with synchrotron radiation, because it provides us the photon energy and light polarization tunability to readily identify molecular levels. Confirmation of the nature of the probed molecular orbitals is obtained by comparing valence band spectra measured at different excitation energies. The analysis relies on the change of photoionization cross section,[40] whose decrease with increasing photon energy is much larger for the valence band features arising from C 2p and N 2p atomic orbitals than for those arising from the 3d atomic orbitals of the Pc metal center, thus changing their relative intensities.[41,42] The inset of Figure 2a depicts F_{16}CuPc on Ag(111) valence band spectra measured with photon energies of 21 and 140 eV, after subtraction of the corresponding substrate reference. The various features are separately labeled, and the spectra are normalized to a common intensity of peak A, which corresponds to the macrocycle-based HOMO (a_{1u} symmetry) composed mainly by C $2p_z$ orbitals. Peak A′ remains almost unchanged, indicating

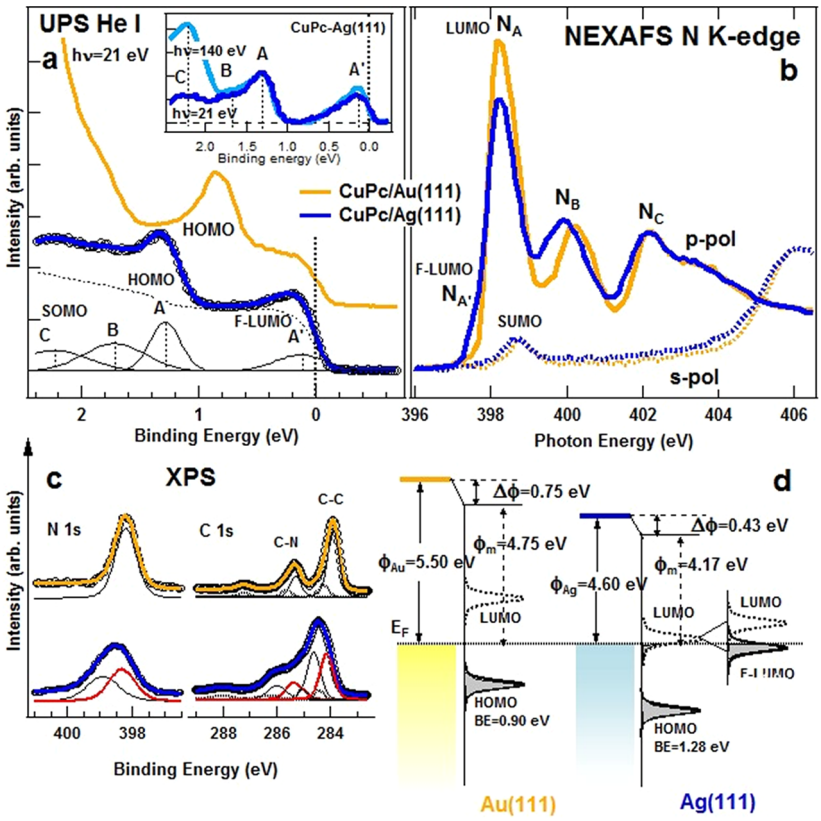

Figure 5. (a) Valence band spectra of CuPc/Au(111) (yellow line) and CuPc/Ag(111) (dark blue line) measured with $h\nu = 21$ eV. For the latter, the fit components (black solid lines) and the Shirley background convoluted with a Fermi step function (black dashed line) obtained from the fitting procedure are shown below. Inset: Valence spectra of CuPc/Ag(111) taken with $h\nu = 21$ eV (dark blue line) and $h\nu = 140$ eV (light blue line) after subtracting the correspondent clean reference spectra. (b) NEXAFS N K-edge spectra of CuPc/Au(111) (yellow line) and CuPc/Ag(111) (dark blue line) acquired under p-polarization (solid lines) and s-polarization (dashed lines). (c) X-ray photoemission spectra in the N 1s (left panels) and C 1s (right panels) core-level regions of CuPc/Au(111) (top spectra) and CuPc/Ag(111) (bottom spectra). Experimental points (markers) are superimposed to fit spectra (solid line). As in Figure 4, the split-off components arising from the partial LUMO filling are colored in red. (d) Energy-level diagrams for CuPc/Au(111) and CuPc/Ag(111). For the latter, E_F crosses the low-energy LUMO tail, inducing a partial charge transfer from substrate to CuPc and the splitting of the two-fold degenerate CuPc LUMO levels.

that both states derive from orbitals with a similar atomic character, such as C or N derived orbitals. This is in line with our suggested scenario of A′ corresponding to a partially filled LUMO orbital and not to the partial filling of the Cu 3d derived singly unoccupied molecular orbital (SUMO).[28] On the other hand, the increasing intensity in the 140 eV spectrum of feature C and partially of feature B [which corresponds to a sum of the vibronic loss of the HOMO (peak A) and the split-off band of state C, as observed for CuPc on Ag(111)[39]] suggests that these signals include contributions from Cu derived orbitals. We therefore ascribe C to the singly occupied molecular orbital (SOMO, b_{1g} symmetry), composed mainly by a Cu $3d_{x^2-y^2}$ orbital mixed with contributions from the in-plane $2p_{x,y}$ orbitals of the four surrounding N atoms.[28]

Regarding the empty molecular states, we obtain important information from the strong linear dichroism exhibited by the NEXAFS spectra (Figure 2b).[43] Low-energy resonances are dominated by transitions into π^* orbitals, whose intensity is maximized under p-polarization and vanishes under s-polarization. Only one small peak is detected in s-polarization at low photon energies. This spectral feature corresponds to transitions from N 1s core levels on the inner nitrogen atoms to those atomic N $2p_{x,y}$ orbitals contributing, together with the Cu $3d_{x^2-y^2}$ orbital, to the SUMO.[28] Its slightly higher energy with respect to the main p-polarization resonance completes, together with the previous photoemission results, our deduction of the sequence of molecular orbitals on Ag(111). As shown in the inset of Figure 2b, the SOMO and SUMO are both outside the HOMO−LUMO gap. The same molecular orbital order is concluded for CuPc on Ag(111) from our combined photon-energy-dependent photoemission spectra (inset in Figure 5a) and NEXAFS experiments (Figure 5b). This goes against several theoretical predictions,[28,32,41] a discrepancy that has been proposed to be related to final state effects in the ionization process.[41,44] However, while this could apply for the SOMO measured by photoemission, that is not the case for the SUMO as probed by non-ionizing NEXAFS transitions. On the other hand, other calculations including stronger electron correlations reproduce the

order concluded from our measurements in the cases of CuPc[42,45] and F_{16}CuPc.[46] Regardless of the above discussion, most important for the present work is that calculations and experiments alike confirm that the charge transfer from substrate to the molecules does not flow into the SUMO but into the degenerate LUMO levels, thereby causing their Jahn–Teller splitting.

The relation of the double core-level components with the observations in NEXAFS spectra needs to be clarified. Split core levels can arise from initial or final state effects. The former might relate to, for example, the presence of different adsorption sites. The increasing number of components in C K-edge and N K-edge NEXAFS spectra could then be interpreted as a result of the double number of initial states for absorption transitions, without invoking the splitting of LUMO levels. However, this should affect transitions into all unoccupied states alike, while unambiguous splitting is observed only in those transitions involving the phthalocyanine's LUMO. Besides, according to this assumption, the equal intensity of the split components in XPS spectra would indicate the presence of two equally populated and well-defined initial states, which in turn imply ordered molecular arrangements. Focusing, for example, on the case of CuPc/Ag(111), the core-level splitting observed in our data (Figure 5c and Figure S2) would point to an ordered structure already at the submonolayer coverage. However, this interpretation goes against reports of Kroger *et al.*, who observe that CuPc molecules at low submonolayer coverage display no crystalline order and behave like a 2D gas at room temperature,[39] discarding again the hypothesis that the splitting of core levels is an initial state effect and causes the doubling of NEXAFS transitions.

We suggest an alternative interpretation that does not contradict the observations above: a lifted degeneracy of the LUMO level upon partial charging in combination with core-hole screening effects as the origin of the doubled core levels. The latter are related to the different screening associated with the delocalized charge throughout the LUMO. As displayed in Figure 1c, the degenerate LUMO levels extend along different molecular diagonals, and partial charging of one of them affects half of each of the atomic species in the molecule [this effect is not observed on the F atoms, which as shown in Figure 1c hardly participate of the LUMO level and therefore leave its core levels virtually unaffected (Figure S3)]. While the split core-level components at higher binding energy nearly follow the work function shift of the system, their counterparts benefit from the more effective screening of the partially filled LUMO and are found at lower binding energy. The efficiency of electron screening depends on the degree of LUMO filling; that is, major screening effects are observed for the system with the largest amount of transferred charge. This is again the case of F_{16}CuPc:PEN/Cu(111), where the energy separation of the core-level doublets is largest in both C 1s and N 1s spectra. Because NEXAFS transitions do not ionize the molecules, screening hardly affects the absorption spectra and the splitting can be directly ascribed to the lifted degeneracy of the LUMO levels.

Proof and direct observation of the Jahn–Teller effect upon phthalocyanine charging has been obtained by scanning tunneling microscopy and spectroscopy on CuPc charged externally by the scanning probe.[27] The LUMO splitting was claimed to amount to 0.21 eV, and although this value is significantly smaller than the ~0.7 eV estimated from the analysis of Figure 5 (~0.55 eV between main and side maxima in NEXAFS spectra, plus 0.15 eV binding energy of the F-LUMO intensity maximum in the valence band spectrum), this discrepancy might arise from the different characterization techniques, as well as from the effect of considerably different substrates [an insulating NaCl bilayer on Cu(111) in ref 27 *vs* Ag(111) in the present work]. Overall, the observed Jahn–Teller effect in singly charged CuPc molecules provides strong support for our interpretation of the spectroscopic fingerprints upon partial charge transfer to CuPc and F_{16}CuPc.

CONCLUSIONS

In this work, we show how the energy-level alignment of semiconducting molecules on metal surfaces can be tailored by an appropriate control of the substrate's work function. Beyond the commonly applied approaches of work function manipulation (addition of buffer layers, changing the substrate material or surface orientation), we demonstrate control of the interface energetics for one given molecule–substrate combination in intimate contact. We do so appropriately modifying the molecule's supramolecular environment. Taking copper phthalocyanines as test molecules, we can even trigger partial charge transfer into their unoccupied molecular orbitals. Furthermore, our detailed spectroscopic analysis reveals that as a result of such charge transfer the phthalocyanine's LUMO degeneracy is lifted by a Jahn–Teller effect, breaking the four-fold symmetry of the molecule and leaving clearly recognizable spectroscopic fingerprints.

METHODS

The Au(111), Ag(111), and Cu(111) surfaces were prepared by standard Ar sputtering and annealing cycles, and their cleanliness was checked by XPS or STM prior to molecular deposition. CuPc, F_{16}CuPc, and PEN were purchased from Sigma-Aldrich. The molecules have been used as received, except F_{16}CuPc, which was additionally purified by gradient sublimation. The molecular layers were prepared by the deposition from

resistively heated Knudsen cells at temperatures around 380 and 190 °C for the phthalocyanines and pentacene, respectively, onto single-crystal surfaces held at room temperature. The sample coverage was monitored by means of a quartz crystal microbalance and further corroborated by detailed analysis of the relative core-level peak intensities. Potential beam damage on the films was minimized by moving the photon beam across the sample during long-lasting measurements. Beam damage as the source of spectral changes was nevertheless checked and discarded by testing the reproducibility of spectra after irradiation.

All measurements were performed at room temperature under ultrahigh vacuum conditions. NEXAFS and XPS experiments were performed at the ALOISA beamline of the synchrotron light source ELETTRA in Trieste (Italy). NEXAFS spectra were taken in partial electron yield by means of a channeltron detector. Spectra measured at the C and N K-edges were calibrated by acquisition of the 1s$-\pi^*$ gas phase transitions of CO and N_2 at $h\nu$ = 287.4 and 401.10 eV, respectively.[47] The manipulator is coaxial to the photon beam, which allows one to change the orientation of the surface with respect to linear polarization of the beam while keeping the grazing angle constant, that is, without changing the beam footprint on the sample. For more details about the scattering geometry, see ref 48. In order to compare the intensity of the spectra taken on the different samples, the spectra have been normalized to the intensity at high photon energy (*i.e.*, $h\nu$ = 305 eV for the C K-edge and $h\nu$ = 420 eV for the N K-edge).

The XPS data were collected by means of a hemispherical electron energy analyzer in normal emission while keeping the sample at grazing incidence (~4°), with excitation energies of 140 eV (valence band) and 530 eV (C 1s, N 1s) and overall resolution of 120 and 240 meV, respectively. The binding energy of core-level spectra is carefully calibrated taking the substrate core-level energies as absolute references. The fitting of all XPS spectra was done using a Shirley background and Voigt integral functions. In all C 1s and N 1s spectra, the Lorentzian width, fwhm, and BE intensity ratio among the different components are left as free parameters of the fit. In C 1s and N 1s spectra of F_{16}CuPc/Ag(111) and F_{16}CuPc:PEN/Cu(111), the intensity ratio of the double components results close to unity within 15%.

Ultraviolet photoemission spectroscopy measurements were recorded at 45° off-normal emission.Valence band spectra of F_{16}CuPc/Au(111) and F_{16}CuPc/Ag(111) were measured using the He I line (21.2 eV) from a non-monochromatized gas discharge lamp and a SPECS Phoibos 100 electron analyzer. The He I satellite lines (β and γ) caused by the non-monochromatized photon source were also taken into account by reducing the intensity of the spectra by 2 and 0.4% at fixed kinetic energy intervals of 1.87 and 2.52 eV, respectively, from the emission associated with the He I α main line. This data treatment removes the substrate d-band satellites in the vicinity of the photoemission peaks of F_{16}CuPc. The fit procedure of the valence band spectra was then made using a Shirley background and Voigt integral functions. Valence band spectra of monolayers and blends on Cu(111) were acquired using the He I α line from a monochromatized gas discharge lamp and a SPECS Phoibos 150 electron analyzer with energy and angle resolutions of ≈40 meV and 0.1°, respectively.

The work function was determined by the low-energy cutoff in the photoemission spectra (sample bias 24 V). STM images were measured at room temperature in a commercial JEOL STM system in constant current mode. The analysis of the STM images has been performed with the freeware WSxM from Nanotec.[49] Calculation details regarding the displayed molecular orbitals of F_{16}CuPc are provided in ref 32.

Conflict of Interest: The authors declare no competing financial interest.

Acknowledgment. This work was supported by the Spanish Grant Nos. MAT2010-21156-C03-01, PIB2010US-00652, and the Basque Government Grant No. IT-621-13. We acknowledge funding from the European Community's Seventh Framework Programme (FP7/2007-2013) under Grant No. 226716. We thank J.-M. Garcia-Lastra for interesting discussions, G. Lovat, A. Verdini, and A. Cossaro for their support during beamtimes, Y. Wakayama for his support with STM measurements, and D. Pickup for his help with home-laboratory photoemission measurements.

Supporting Information Available: Data on F_{16}CuPc multilayer films in comparison with the various monolayers discussed in the article (Figure S1), the evolution of core levels and valence band photoemission spectra from CuPc submonolayer to multilayer coverage (Figure S2), and F 1s core levels for the various monolayers discussed in the article (Figure S3). This material is available free of charge *via* the Internet at http://pubs.acs.org.

REFERENCES AND NOTES

1. Marmont, P.; Battaglini, N.; Lang, P.; Horowitz, G.; Hwang, J.; Kahn, A.; Amato, C.; Calas, P. Improving Charge Injection in Organic Thin-Film Transistors with Thiol-Based Self-Assembled Monolayers. *Org. Electron.* **2008**, *9*, 419–424.
2. Ziroff, J.; Foster, F.; Schöll, A.; Puschnig, P.; Reinert, F. Hybridization of Organic Molecular Orbitals with Substrate States at Interfaces: PTCDA on Silver. *Phys. Rev. Lett.* **2010**, *104*, 233004.
3. Heimel, G.; Duhm, S.; Salzmann, I.; Gerlach, A.; Strozecka, A.; Niederhausen, J.; Burker, C.; Hokosai, T.; Fernandez-Torrente, I.; Schulze, G.; *et al.* Charged and Metallic Molecular Monolayers through Surface-Induced Aromatic Stabilization. *Nat. Chem.* **2013**, *5*, 187–194.
4. Salzmann, I.; Heimel, G.; Duhm, S.; Oehzelt, M.; Pingel, P.; George, B. M.; Schneeg, A.; Lips, K.; Blum, R.-P.; Vollmer, A.; *et al.* Intermolecular Hybridization Governs Molecular Electrical Doping. *Phys. Rev. Lett.* **2012**, *108*, 035502.
5. Koch, N.; Duhm, S.; Rabe, J. P.; Vollmer, A.; Johnson, R. L. Optimized Hole Injection with Strong Electron Acceptors at Organic–Metal Interfaces. *Phys. Rev. Lett.* **2005**, *95*, 237601.
6. Tseng, C.-T.; Cheng, Y.-H.; Lee, M.-C. M.; Han, C.-C.; Cheng, C.-H.; Tao, Y.-T. Study of Anode Work Function Modified by Self-Assembled Monolayers on Pentacene/Fullerene Organic Solar Cells. *Appl. Phys. Lett.* **2007**, *91*, 233510.
7. Hong, J.-P.; Park, A.-Y.; Lee, S.; Kang, J.; Shin, N.; Yoon, D. Y. Tuning of Ag Work Functions by Self-Assembled Monolayers of Aromatic Thiols for an Efficient Hole Injection for Solution Processed Triisopropylsilylethynyl Pentacene Organic Thin Film Transistors. *Appl. Phys. Lett.* **2008**, *92*, 143311.
8. Jia, Z.; Lee, V. W.; Kymissis, I.; Floreano, L.; Verdini, A.; Cossaro, A.; Morgante, A. *In Situ* Study of Pentacene Interaction with Archetypal Hybrid Contacts: Fluorinated *versus* Alkane Thiols on Gold. *Phys. Rev. B* **2010**, *82*, 125457.
9. Monch, W. On the Physics of Metal–Semiconductor Interfaces. *Rep. Prog. Phys.* **1990**, *53*, 221–278.
10. Tung, R. T. The Physics and Chemistry of the Schottky Barrier Height. *Appl. Phys. Rev.* **2014**, *1*, 011304.
11. Hwang, J.; Wan, A.; Kahn, A. Energetics of Metal–Organic Interfaces: New Experiments and Assessment of the Field. *Mater. Sci. Eng. R* **2009**, *64*, 1–31.
12. Flores, F.; Ortega, J.; Vazquez, H. Modelling Energy Level Alignment at Organic Interfaces and Density Functional Theory. *Phys. Chem. Chem. Phys.* **2009**, *11*, 8658–8675.
13. Gonzalez-Lakunza, N.; Fernandez-Torrente, I.; Franke, K. J.; Lorente, N.; Arnau, A.; Pascual, J. I. Formation of Dispersive Hybrid Bands at an Organic–Metal Interface. *Phys. Rev. Lett.* **2008**, *100*, 156805.
14. Franke, K. J.; Schulze, G.; Henningsen, N.; Fernandez-Torrente, I.; Pascual, J. I.; Zarwell, S.; Ruck-Braun, K.; Cobian, M.; Lorente, N. Reducing the Molecule–Substrate Coupling in C60-Based Nanostructures by Molecular Interactions. *Phys. Rev. Lett.* **2008**, *100*, 036807.
15. de Oteyza, D. G.; Silanes, I.; Ruiz-Oses, M.; Barrena, E.; Doyle, B. P.; Arnau, A.; Dosch, H.; Wakayama, Y.; Ortega, J. E. Balancing Intermolecular and Molecule–Substrate Interactions in Supramolecular Assemblies. *Adv. Funct. Mater.* **2009**, *19*, 259–264.
16. de Oteyza, D. G.; Garcia-Lastra, J. M.; Corso, M.; Doyle, B. D.; Floreano, L.; Morgante, A.; Wakayama, Y.; Rubio, A.; Ortega,

J. E. Customized Electronic Coupling in Self-Assembled Donor–Acceptor Nanostructures. *Adv. Funct. Mater.* **2009**, *19*, 3567–3563.
17. El-Sayed, A.; Mowbray, D. J.; Garcia-Lastra, J. M.; Rogero, C.; Goiri, E.; Borghetti, P.; Turak, A.; Doyle, B. P.; Dell'Angela, M.; Floreano, L.; *et al.* Supramolecular Environment-Dependent Electronic Properties of Metal–Organic Interfaces. *J. Phys. Chem. C* **2012**, *116*, 4780–4785.
18. Cabellos, J. L.; Mowbray, D. J.; Goiri, E.; El-Sayed, A.; Floreano, L.; de Oteyza, D. G.; Rogero, C.; Ortega, J. E.; Rubio, A. Understanding Charge Transfer in Donor–Acceptor/Metal Systems: A Combined Theoretical and Experimental Study. *J. Phys. Chem. C* **2012**, *116*, 17991–18001.
19. El-Sayed, A.; Borghetti, P.; Goiri, E.; Rogero, C.; Floreano, L.; Lovat, G.; Mowbray, D. J.; Cabellos, J. L.; Wakayama, Y.; Rubio, A.; *et al.* Understanding Energy Level Alignment in Donor–Acceptor/Metal Interfaces from Core-Level Shifts. *ACS Nano* **2013**, *7*, 6914–6920.
20. Goiri, E.; Matena, M.; El-Sayed, A.; Lobo-Checa, J.; Borghetti, P.; Detlefs, B.; Duvernay, J.; Ortega, J. E.; de Oteyza, D. G. Self-Assembly of Bicomponent Molecular Monolayers: Adsorption Height Changes and Their Consequences. *Phys. Rev. Lett.* **2014**, *112*, 117602.
21. Zhong, J.-Q.; Qin, X.; Zhang, J.-L.; Kera, S.; Ueno, N.; Wee, A. T. S.; Yang, J.; Chen, W. Energy Level Realignment in Weakly Interacting Donor–Acceptor Binary Molecular Networks. *ACS Nano* **2014**, *8*, 1669–1707.
22. Stadtmuller, B.; Luftner, D.; Willenbockel, M.; Reinisch, E. M.; Sueyoshi, T.; Koller, G.; Soubatch, S.; Ramsey, M. G.; Puschnig, P.; Tautz, S.; *et al.* Unexpected Interplay of Bonding Height and Energy Level Alignment at Heteromolecular Hybrid Interfaces. *Nat. Commun.* **2014**, *5*, 3685.
23. Peisert, H.; Knupfer, M.; Schwieger, T.; Fuentes, G. G.; Olligs, D.; Fink, J.; Schmidt, Th. Fluorination of Copper Phthalocyanines: Electronic Structure and Interface Properties. *J. Appl. Phys.* **2003**, *93*, 9683–9692.
24. Yan, L.; Watkins, N. J.; Zorba, S.; Gao, Y. Thermodynamic Equilibrium and Metal–Organic Interface Dipole. *Appl. Phys. Lett.* **2002**, *81*, 2752–2754.
25. Kahn, A.; Koch, N.; Gao, W. Electronic Structure and Electrical Properties of Interfaces between Metals and Conjugated Molecular Films. *J. Polym. Sci., Part B: Polym. Phys.* **2003**, *41*, 2529–2548.
26. Zahn, D. R. T.; Gavrila, G. N.; Gorgoi, M. The Transport Gap of Organic Semiconductors Studied Using the Combination of Direct and Inverse Photoemission. *Chem. Phys.* **2006**, *325*, 99–112.
27. Uhlmann, C.; Swart, I.; Repp, J. Controlling the Orbital Sequence in Individual Cu-Phthalocyanine Molecules. *Nano Lett.* **2013**, *13*, 777–780.
28. Piper, L. F. J.; Cho, S. W.; Zhang, Y.; DeMasi, A.; Smith, K. E.; Matsuura, A. Y.; McGuinness, C. Soft X-ray Spectroscopy Study of the Element and Orbital Contributions to the Electronic Structure of Copper Hexadecafluoro-Phthalocyanine. *Phys. Rev. B* **2010**, *81*, 045201.
29. Calabrese, A.; Floreano, L.; Verdini, A.; Mariani, C.; Betti, M. G. Filling Empty States in a CuPc Single Layer on the Au(110) Surface *via* Electron Injection. *Phys. Rev. B* **2009**, *79*, 115446.
30. Evangelista, F.; Gotter, R.; Mahne, N.; Nannarone, S.; Ruocco, A.; Rudolf, P. Electronic Properties and Orbital-Filling Mechanism in Rb-Intercalated Copper Phthalocyanine. *J. Phys. Chem. C* **2008**, *112*, 6509–6514.
31. Wakayama, Y.; de Oteyza, D. G.; Garcia-Lastra, J. M.; Mowbray, D. J. Solid-State Reactions in Binary Molecular Assemblies of F_{16}CuPc and Pentacene. *ACS Nano* **2011**, *5*, 581–589.
32. de Oteyza, D. G.; El-Sayed, A.; Garcia-Lastra, J. M.; Goiri, E.; Krauss, T. N.; Turak, A.; Barrena, E.; Dosch, H.; Zegenhagen, J.; Rubio, A.; *et al.* Copper-Phthalocyanine Based Metal–Organic Interfaces: The Effect of Fluorination, the Substrate, and Its Symmetry. *J. Chem. Phys.* **2010**, *133*, 214703.
33. Koch, N.; Gerlach, A.; Duhm, S.; Glowatzki, H.; Heimel, G.; Vollmer, A.; Sakamoto, Y.; Suzuki, T.; Zegenhagen, J.; Rabe, J. P.; *et al.* Adsorption-Induced Intramolecular Dipole: Correlating Molecular Conformation and Interface Electronic Structure. *J. Am. Chem. Soc.* **2008**, *130*, 7300–7304.
34. Gonzalez-Lakunza, N.; Canas-Ventura, M. E.; Ruffieux, P.; Rieger, R.; Mullen, K.; Fasel, R.; Arnau, A. Hydrogen-Bonding Fingerprints in Electronic States of Two-Dimensional Supramolecular Assemblies. *ChemPhysChem* **2009**, *10*, 2943–2946.
35. Fernandez-Torrente, I.; Franke, K. J.; Pascual, J. I. Spectroscopy of C60 Single Molecules: The Role of Screening on Energy Level Alignment. *J. Phys.: Condens. Matter* **2008**, *20*, 184001.
36. Gerlach, A.; Schreiber, F.; Sellner, S.; Dosch, H.; Vartanyants, I. A.; Cowie, B. C. C.; Lee, T.-L.; Zegenhagen, J. Adsorption-Induced Distortion of F_{16}CuPc on Cu(111) and Ag(111): An X-ray Standing Wave Study. *Phys. Rev. B* **2005**, *71*, 205425.
37. Kroger, I.; Stadtmuller, B.; Kleimann, C.; Rajput, P.; Kumpf, C. Normal-Incidence X-ray Standing-Wave Study of Copper Phthalocyanine Submonolayers on Cu(111) and Au(111). *Phys. Rev. B* **2011**, *83*, 195414.
38. Babudri, F.; Farinola, G. M.; Naso, F.; Ragni, R. Fluorinated Organic Materials for Electronic and Optoelectronic Applications: The Role of the Fluorine Atom. *Chem. Commun.* **2007**, 1003–1022.
39. Kroger, I.; Stadtmuller, B.; Stadler, C.; Ziroff, J.; Kochler, M.; Stahl, A.; Pollinger, F.; Lee, T.-L.; Zegenhagen, J.; Reinert, F.; *et al.* Submonolayer Growth of Copper-Phthalocyanine on Ag(111). *New J. Phys.* **2010**, *12*, 083038.
40. Yeh, J. J.; Lindau, I. Atomic Subshell Photoionization Cross Sections and Asymmetry Parameters. *At. Data Nucl. Data Tables* **1985**, *32*, 1–155.
41. Evangelista, F.; Carravetta, V.; Stefani, G.; Jansik, B.; Alagia, M.; Stranges, S.; Ruocco, A. Electronic Structure of Copper Phthalocyanine: An Experimental and Theoretical Study of Occupied and Unoccupied Levels. *J. Chem. Phys.* **2007**, *126*, 124709.
42. Nardi, M. V.; Detto, F.; Aversa, L.; Verucchi, R.; Salviati, G.; Iannotta, S.; Casarin, M. Electronic Properties of CuPc and H_2Pc: An Experimental and Theoretical Study. *Phys. Chem. Chem. Phys.* **2013**, *15*, 12864–12881.
43. de Oteyza, D. G.; Sakko, A.; El-Sayed, A.; Goiri, E.; Floreano, L.; Cossaro, A.; Garcia-Lastra, J. M.; Rubio, A.; Ortega, J. E. Inversed Linear Dichroism in F K-Edge NEXAFS Spectra of Fluorinated Planar Aromatic Molecules. *Phys. Rev. B* **2012**, *86*, 075469.
44. Liao, M.-S.; Scheiner, S. Electronic Structure and Bonding in Metal Phthalocyanines, Metal = Fe, Co, Ni, Cu, Zn, Mg. *J. Chem. Phys.* **2001**, *114*, 9780–9791.
45. Aristov, V. Y.; Molodtsova, O. V.; Maslyuk, V.; Vyalikh, D. V.; Zhilin, V. M.; Ossipyan, Y. A.; Bredow, T.; Mertig, I.; Knupfer, M. Electronic Structure of Pristine CuPc: Experiment and Calculations. *Appl. Surf. Sci.* **2007**, *254*, 20–25.
46. Ren, J.; Meng, S.; Wang, Y.-L.; Ma, X.-C.; Xue, Q.-K.; Kaxiras, E. Properties of Copper (Fluoro-)phthalocyanine Layers Deposited on Epitaxial Graphene. *J. Chem. Phys.* **2011**, *134*, 194706.
47. Floreano, L.; Naletto, G.; Gvetko, D.; Gotter, R.; Malvezzi, M.; Marassi, L.; Morgante, A.; Santaniello, A.; Verdini, A.; Tommasini, F.; *et al.* Performance of the Grating-Crystal Monochromator of the ALOISA Beamline at the Elettra Synchrotron. *Rev. Sci. Instrum.* **1999**, *70*, 3855–3864.
48. Floreano, L.; Cossaro, A.; Gotter, R.; Verdini, A.; Bavdek, G.; Evangelista, F.; Ruocco, A.; Morgante, A.; Cvetko, D. Periodic Arrays of Cu-Phthalocyanine Chains on Au(110). *J. Phys. Chem. C* **2008**, *112*, 10794–10802.
49. Horcas, I.; Fernandez, R.; Gomez-Rodriguez, J. M.; Colchero, J.; Gomez-Herrero, J.; Baro, A. M. WSXM: A Software for Scanning Probe Microscopy and a Tool for Nanotechnology. *Rev. Sci. Instrum.* **2007**, *78*, 013705.